Rotational dynamics of semiflexible paramagnetic particle chains

Sibani Lisa Biswal
Department of Chemical Engineering, Stanford University, Stanford, California 94305, USA

Alice P. Gast*
Department of Chemical Engineering, Massachusetts Institute of Technology, Cambridge, Massachusetts 02139, USA
(Received 1 October 2003; published 30 April 2004)

Paramagnetic particles have the unique ability to reversibly form magnetic chains. We have taken advantage of this property by permanently linking the chains with three linking chemistries to create flexible chains whose behavior changes with the application of a magnetic field. We study the behavior of these chains in a rotating magnetic field and model them as elastic rods. Rigid chains rotate as a solid body while flexible chains deform under the influence of magnetic, viscous, and elastic stresses. We find that the shapes chains assume in rotating magnetic fields confirm the chain flexibility determined from previous micromechanics measurements.

DOI: 10.1103/PhysRevE.69.041406 PACS number(s): 82.70.Dd

I. INTRODUCTION

Magnetorheological (MR) fluids are a special class of "tunable" fluids consisting of paramagnetic colloidal particles in a nonmagnetic liquid. MR fluids form reversible chain and network structures under the influence of an external magnetic field. In the absence of an external magnetic field, these particles are randomly distributed due to thermal motion. Once a magnetic field is applied, the particles acquire dipole moments causing them to aggregate to form chains in the field direction. This ability to rapidly and reversibly change behavior has made these particles useful in devices such as tunable dampers and brakes [1,2].

There have been several studies of the behavior of MR fluids in a continuously rotating field [3,4]. Paramagnetic particles respond to an external rotating magnetic field by forming chains that rotate into magnetic alignment at a rate that depends upon the viscosity of the medium. Some researchers have taken advantage of this property to probe the microrheology and viscoelastic properties of suspensions [5,6]. As the frequency of the external magnetic field increases, the chains rupture in response to the increasing viscous drag force acting on them. Paramagnetic particle chains sometimes form interesting "S"- and "U"-like shapes before breaking at high frequencies [7,8].

In this paper, we examine the behavior of permanently linked semiflexible chains of particles that cannot rupture under viscous drag. Instead, these chains deform in response to an increase in the frequency of a rotating magnetic field.

A variety of linking chemistries can be used to create permanently linked chains of magnetic particles. We use a symmetric bifunctional molecule that reacts with the complementary functional group on the paramagnetic particle. Linked chains can be synthesized by forming covalent bonds between neighboring amine-functionalized microspheres with gluteraldehyde [9]. We also create chains by linking paramagnetic particles with a flexible poly-ethylene-glycol (PEG) spacer molecule as described before [10]. Using optical tweezers, we subjected the chains to bending and stretching forces to determine the flexural rigidity, or bending stiffness, of the chain. We have shown that changing the length of the spacer molecule allows us to tune the chain flexibility.

In a rotating magnetic field, the chains are subjected to a load force increasing linearly along the chain such that the chains are elastically deformed into S shapes. We examine the resulting chain curvature using our previously determined flexural rigidity values [10]. We also investigate the buckling and folding that occurs under some conditions.

Magnetically actuating these linked chains in microchannels provides a unique means to manipulate microfluidic flows; rotating linked chains can serve as miniature stir bars to mix fluids. Also, microcircuits have been developed to generate magnetic fields on microfluidic chips to move paramagnetic particles [11]. These circuits enable the creation of very small magnetically activated systems.

II. THEORY

A. Paramagnetic particles

The paramagnetic particles are polystyrene microspheres with iron oxide grains embedded within them. When an external magnetic field of magnitude H_o is applied, the particles acquire an induced dipole moment, $\mu = \frac{4}{3}\pi a^3 \mu_o \chi H_o$, where a and χ are the particle radius and susceptibility, and μ_o is the magnetic permeability of a vacuum. Two particles with aligned dipole moments will have an interaction energy given by

$$U_{mag}(r,\alpha) = \frac{\mu^2}{4\pi\mu_o}\frac{(1-3\cos^2\alpha)}{r^3}, \tag{1}$$

where r is the distance between sphere centers and α is the angle between the applied field and the sphere centers. The magnetic force between particles is

*Electronic address: gast@mit.edu

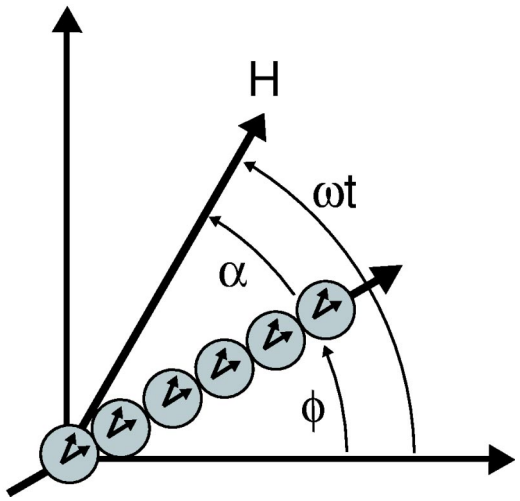

FIG. 1. Geometry of a chain in a rotating external magnetic field.

$$\vec{F}_{mag} = \frac{3\mu^2}{4\pi\mu_o r^4}(3\cos^2\alpha - 1)\hat{r} + \frac{3\mu^2}{4\pi\mu_o r^4}\sin(2\alpha)\hat{\theta}. \quad (2)$$

The strength of the interaction can be characterized by the dimensionless dipole strength,

$$\lambda = \frac{\pi\mu_o a^3 \chi^2 H_o^2}{9k_b T} \quad (3)$$

defined by the ratio of the maximum interaction energy between two particles aligned with the external magnetic field to the thermal energy.

B. Angular chain motion

To describe the mechanical response of rotating linked magnetic chains we consider a linear chain of N particles of length $L=2Na$. The angular motion of the chain is governed by the balance between the imposed magnetic torque and the viscous torque generated by the motion of the chain through the fluid. When a rotating magnetic field is applied, the dipole interaction generates a magnetic torque on the chain,

$$\Gamma_m = \vec{\mu} \times \vec{H}, \quad (4)$$

causing it to follow the rotating magnetic field. The geometry of the system is shown in Fig. 1. The magnetic field $\vec{H}$ at time t is directed along the angle ωt. The phase lag angle $\alpha = \omega t - \varphi$ between the chain and $\vec{H}$ creates a magnetic torque per volume. A useful quantity to consider when studying the motions of these chains is the Mason number

$$\mathrm{Mn} = \frac{32\eta\omega}{\mu_o \chi^2 H_o^2} \quad (5)$$

defined by the ratio of viscous to magnetic forces on a chain. The Mason number is related to λ defined in Eq. (3) by means of the chain Péclet number Pe defined by the ratio of viscous to thermal forces on the chain:

$$\mathrm{Pe} = \lambda \mathrm{Mn} = \frac{32\pi\eta\omega a^3}{9k_b T}. \quad (6)$$

The torque generated by the magnetic field is counterbalanced by the sum of the following: the torque due to inertia; the viscous drag torque; the elastic torque due to the ends of the chain bending away from the center; and the thermal Brownian torque. Our experiments take place at scales with lengths L in tens of microns, rotational velocities ω in the upper range of 1 Hz, and the kinematic viscosity ν of water of 10^6 $\mu\mathrm{m}^2/\mathrm{sec}$. Therefore, the Reynolds number for our experiment is $\omega a L/\nu \sim 10^{-4}$. Since we operate in dilute suspensions at low Reynolds number, the inertial torque may be neglected and chain-chain interactions are ignored. Additionally, we use a magnetic field strength of 1000 A/m resulting in a Mn that varies between 10 and 50 and $\lambda \sim 4$. The characteristic values of the Pe in these experiments will be in the range of $40 < \mathrm{Pe} < 200$. Since we are at high Pe, viscous forces dominate thermal forces. Therefore, to understand the behavior of linked chains in a rotating magnetic field, we consider the relative strengths of the elastic, viscous, and magnetic torques acting upon a chain.

The magnetic torque acting on a chain of N spherical magnetic particles has been calculated [3,4,6]:

$$\Gamma_m = \frac{3\mu^2}{4\pi\mu_o}\frac{N^2}{2(2a)^3}\sin(2\alpha) \quad (7)$$

as a sum over the magnetic interactions between nearest neighbors.

For a spherical particle rotating in a medium of viscosity η, Stokes law for the frictional torque is $6\pi\eta a\omega$. Doi and Edwards [12] extended this to a chain of N spherical particles and calculated the viscous torque opposing its rotation with angular velocity ω as

$$\Gamma_v = \zeta_r \omega = \kappa V \eta \omega, \quad (8)$$

where κ is a shape factor and $V = N(4/3)\pi a^3$ is the volume of the chain. The shape factor for a linear chain made up of N beads, including hydrodynamic interactions is

$$\kappa = \frac{2N^2}{\ln(N/2)}. \quad (9)$$

At a steady angular velocity, the two opposing angular torques must balance at the chain center. Therefore, for a given magnetic chain strength and frequency, there will be a defined phase lag between the direction of the external magnetic field and the chain orientation:

$$\sin(2\alpha) = \frac{32N\eta\omega}{\mu_o \chi^2 H_o^2 \ln(N/2)}. \quad (10)$$

The chain rotates synchronously with the field as long as $\sin(2\alpha) < 1$. In this regime, the chain follows $\vec{H}$ and rotates with the same angular frequency ω as $\vec{H}$ and the phase lag is constant. Once the phase lag angle reaches the value of $\alpha = \pi/4$, the magnetic field is not strong enough to keep the chain at an angle $\alpha < \pi/4$, and the chain begins to rotate asynchronously.

As described previously, when a magnetic field is applied, a magnetic dipole moment is induced in the particles causing each particle to also create a magnetic field itself. This causes a local field effect where the field experienced by each particle is the sum of the applied external field and the local field induced by neighboring particles: $\vec{H}=\vec{H}_o+\vec{H}_1$. The consequence of the local field is that the dipoles are not aligned in the direction of the applied field. The local field induced by neighboring dipoles has been previously calculated [14,15] as

$$\vec{H}_1(r)=\frac{3\hat{r}(\vec{\mu}\cdot\hat{r})-\vec{\mu}}{4\pi a^3\ \mu_o}. \tag{11}$$

The induced dipole moment in a particle is

$$\vec{\mu}=\tfrac{4}{3}\pi a^3\mu_o\chi\vec{H}_1. \tag{12}$$

By solving Eqs. (11) and (12) self-consistently for a chain of particles with equal spacing s, the components of the chain dipole moment $\vec{m}$ can be calculated as

$$m_r=\frac{\frac{4}{3}\pi a^3\mu_o\chi H_o\cos\alpha}{1-\frac{\zeta(3)\chi}{2}\left(\frac{2a}{s}\right)^3}, \tag{13}$$

$$m_\theta=\frac{\frac{4}{3}\pi a^3\mu_o\chi H_o\sin\alpha}{1+\frac{\zeta(3)\chi}{4}\left(\frac{2a}{s}\right)^3}, \tag{14}$$

where $\zeta(3)\approx 1.202$ is the Riemann zeta function. The angle between the dipole moment of the chain and the external magnetic field can be determined from the sum of the components. So for $\alpha=0$ and $\alpha=\pi/2$ the magnetic dipoles are aligned with the magnetic field and the difference between the dipole direction and the external field is 0. Meanwhile, at $\alpha=\pi/4$ the difference between the dipole direction and the external field is at a maximum of 3.6°. This causes the magnetic angular force, aligning the particles with the external field, to increase by about 4 %.

C. Chain shape deformation

There are models to describe the rupture of paramagnetic particle chains in a rotating magnetic field due to hydrodynamic and magnetic stresses [13]. We augment these models to include an elastic component to account for the links between the particles.

In a rotating magnetic field, the chain bends about the center of rotation to balance the magnetic and viscous stresses. We have previously shown that PEG-linked chains will deform elastically depending on the applied force and the properties of the linker. Therefore, we can consider the chain to behave as an elastic rod.

For a stable chain shape, the tension induced along the chain by the hydrodynamic stress must balance the radial attractive dipolar magnetic force and the elastic restorative force. A static analysis of the forces applied to a bent chain allows us to calculate the radial hydrodynamic force by summing the drag for each bead along the chain [13]:

$$\vec{F}_d=\sum_{i=-N/2}^{N/2}6\pi\eta a\vec{v}_i, \tag{15}$$

where $\vec{v}_i=\omega r_i\hat{r}$ is the velocity of the ith particle. For a straight chain modeled as a cylinder, $\vec{F}_d=\zeta_\perp\vec{v}_i$ where the translational drag coefficient is

$$\zeta_\perp=\frac{4\pi\eta aN}{\ln(N/2)}. \tag{16}$$

Summing the radial component of the magnetic dipolar force for each bead gives

$$\vec{F}_m=\frac{3\mu^2}{4\pi\mu_o a^4}\sum_{i=-N/2}^{i=N/2}(3\cos^2\alpha_i-1)\hat{r}, \tag{17}$$

where α_i is the phase lag angle for the ith particle. By subtracting the drag force from the magnetic force acting on each particle, we can calculate the elastic force along the length of the chain.

A bent elastic rod exerts a restorative force given by $\vec{F}_{elas}=-dU_{bend}/d\hat{r}$, where the bending energy per unit rod length U_{bend} is related to the chain curvature $d\Theta/ds$ as

$$U_{bend}=\frac{EI}{2}\int_0^L\left(\frac{d\Theta}{ds}\right)^2ds, \tag{18}$$

where EI is the flexural rigidity, Θ is the tangent angle along the chain, and s is the arc length along the chain. The flexural rigidity is a measure of the resistance of an elastic rod to external bending forces. The flexural rigidity can be separated into the Young's modulus E and the moment of inertia, $I=\pi a^4/4$, for a rod with a circular cross section of radius a. The flexural rigidity is directly proportional to the persistence length, $L_p=EI/k_bT$.

The elastic torque per volume due to chain bending is given by $\Gamma_{el}=EI(d^2\Theta/ds^2)$. By considering a static deformation of the chain with small deflections, we can approximate the arc length and curvature by $s\approx x$ and $d\Theta/ds\approx d^2y/dx^2$ with the coordinates x along the unbent chain and y perpendicular to the chain. The force per unit length f acting on a chain can be found by differentiating Eq. (18):

$$f=EI\frac{d^4y}{dx^4}. \tag{19}$$

The viscous load on the rotating chains increases nearly linearly along the chain length, $f=f_mx/L$, with the maximum force density at the ends of the rotating magnetic chain. The reference frame is chosen such that the chain is fixed at the center; therefore, $y(0)=y'(0)=0$. While the ends being free imply that $y''(L)=y'''(L)=0$. Inserting these boundary conditions and $f=0$ at $x=0$ and $f=f_m$ at $x=L$ into Eq. (19) gives the shape of the bent chain:

$$y(x) = \frac{f_m x^5}{120EIL} - \frac{f_m L x^3}{12EI} + \frac{f_m L^2 x^2}{6EI}. \quad (20)$$

III. MATERIALS AND METHODS

We study streptavidin coated paramagnetic latex particles purchased from Seradyn Inc. (Sera-Mag Part 3015-2105, 1 ml, 1 % solids by weight). The particles are polystyrene spheres with 40 wt % magnetite encapsulated by copolymerization with covalently bound streptavidin groups on the surface. The mean particle diameter is $2a=0.78$ μm and the particle susceptibility $\chi=0.67\pm.01$.

The linked chains are prepared as described previously [10]. Briefly, the chains are prepared in a $50\times50\times30$ mm^3 flow cell made from a bovine serum albumin (BSA) (Sigma Chemicals)-coated glass microscope slide attached to a BSA-coated glass coverslip with double-stick tape. The particles are diluted to 0.01 wt % solids in a *pH* 7 borate buffer containing 1 % Tween 20 (Sigma Chemicals). The particles are flowed into the cell and placed in a magnetic field of 30 mT with two permanent magnets to cause them to aggregate into linear chains. We link the particles by reacting the streptavidin molecules on the particle surface with PEG spacer molecules carrying the ligand biotin on both ends. The high affinity of biotin for streptavidin results in stable attachments of the spacer molecules to the particles. We studied chains linked with two bis-biotin-PEG lengths: molecular weight (g/mol) MW=733 (Pierce Chemicals) and MW=3400 (Shearwater Chemicals). The linker is introduced at a concentration of 10 mg/ml in borate buffer to ensure the saturation of the streptavidin sites. The cell is then sealed with epoxy to prevent evaporation.

Additionally, we create more rigid chains with amine-terminated paramagnetic particles purchased from (Spherotech). These particles are also polystyrene spheres with 40 % magnetite with amine groups on the surface. The mean particle diameter is $2a=1.1$ μm and the particle susceptibility $\chi=0.66\pm.09$. Once these particles form chains, a 1 % gluteraldehyde (Polysciences Inc.) is introduced to covalently link them. After $\approx$10 min a 10 % lysine solution (Sigma Chemicals) is added to quench the linking reaction. The flow cell is then sealed with epoxy.

The rotating magnetic field is created by two perpendicular pairs of Helmholtz coils, which generate orthogonal magnetic fields. Each coil is made by winding 1000 turns of 24 gauge copper wire around a ferrite core. A multifrequency synthesizer (HP 8904A) is programmed to provide sinusoidal ac currents through the coils to create a field in the x direction $H_x=H_o\sin(\omega t)$, and in the y direction $H_y=H_o\sin(\omega t+\pi/2)$. This results in a homogeneous magnetic field that rotates in the horizontal plane. The instantaneous direction of the field is monitored using a digital oscilloscope (HP 54501A). Using 10 V, we generate a magnetic field of 1000 A/m. The rotational frequency can be varied from 0.1 to 10 Hz.

The flow cell with the linked chains is placed on a microscope stage (Nikon Diaphot) with a Plan M $100\times/1.2$ objective in the center of the two pairs of coils. We monitor the chain rotations with video microscopy from a digital camera (Hamamatsu) at a rate of 10 frames/sec using Simple PCI software. Images are transferred to image analysis software (Scion Image, NIH public domain software). Image processing includes binarizing the image to obtain pixel coordinates for the centers of each particle using a modified version of Scion Image particle-tracking macro. For a chain at a given frequency, the center of rotation of the chain and the average deformation are determined by overlapping sequential images at a particular frequency. The distances from the center of the rotation to the ends of the chain are measured.

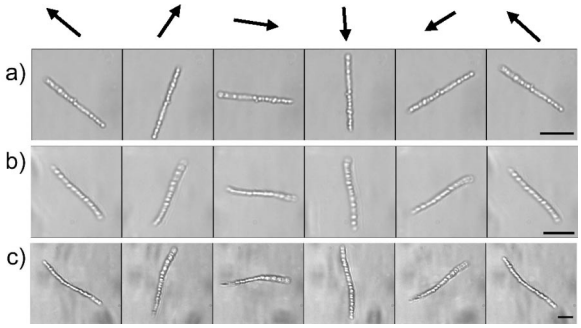

FIG. 2. Linear chains rotating synchronously with a 1000 A/m rotating magnetic field at $f=0.1$ Hz. Frames taken at 0.1 sec intervals. Chains are linked with (a) gluteraldehyde, (b) PEG 733, and (c) PEG 3400. Qualitative differences in chain deformation between the gluteraldehyde-linked and the PEG-linked chains can be seen during chain rotation. The direction of the magnetic field is shown by the black arrows. Scale bar: 10 μm.

IV. RESULTS AND DISCUSSION

All experiments took place at a magnetic field of 1000 A/m or at $\lambda=4$. Chains of 20–100 μm linked with PEG 733, PEG 3400, and gluteraldehyde are studied in a rotating magnetic field at low frequencies, from 0.1 to 0.5 Hz. One can see the qualitative difference in flexibility between the gluteraldehyde-linked chains and the PEG-linked chains by monitoring the chain deformation using video microscopy. Video images of the three different types of rotating chains are shown in Fig. 2. We begin by subjecting various samples to a rotating magnetic field with a frequency of 0.1 Hz. We studied the behavior as the rotational rate is increased in increments of 0.1 Hz.

Typically, there are two regimes of rotational behavior and within each regime there are different chain responses. The simplest is the synchronous regime where the chain follows the external magnetic field with a constant phase lag angle. The other is the asynchronous regime where the phase lag angle increases with time due to the rotational viscous torque preventing the chain from following the external field. Within the synchronous regime, there are chains that fold into a shape with a smaller effective length, reducing the drag and allowing the chains to follow the external field.

We calculate the critical dimensionless chain length where there is a transition between the synchronous and asynchronous regimes for a given Mn by solving Eq. (10) for $\sin(2\alpha)=1$, as shown in Fig. 3(a). For chains shorter than the

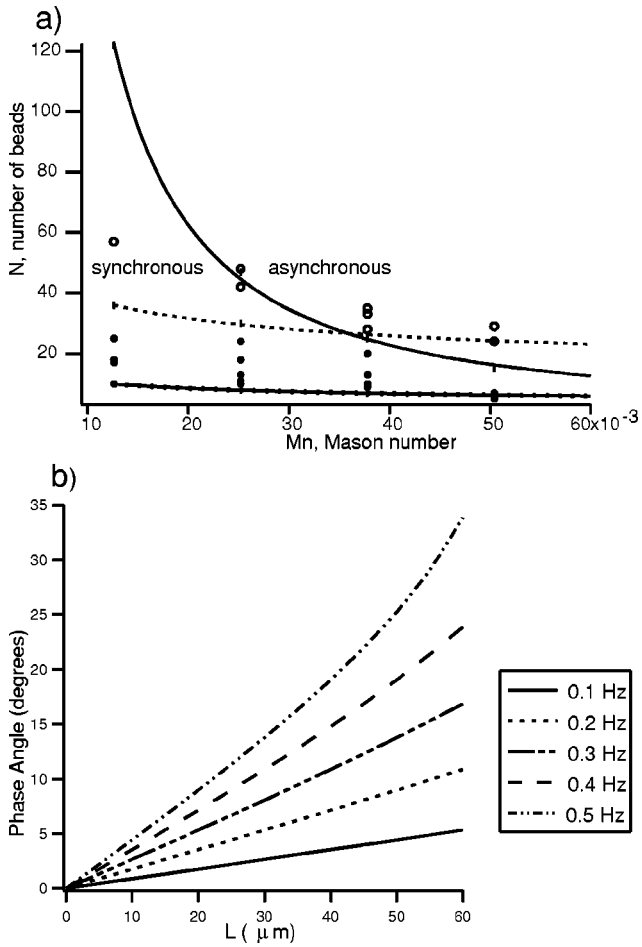

FIG. 3. (a) A plot describing the chain behavior expected for various chains lengths vs Mn. The upper curve shows the threshold for viscous forces to dominate and for chains to go from rotating synchronously to asynchronously. The lower curves show the bounds where viscous forces dominate over elastic forces causing a chain to deform. The elastic forces are calculated using $EI \sim 10^{-21}$ N m^2 shown as the dashed line and $EI \sim 10^{-23}$ N m^2 shown as the dotted line. We have placed our experimental results onto the plot. Filled circles represent a sample where the chains are rotating synchronously. Open circles represent cases of asynchronous rotation. (b) Plot of the calculated phase lag angle of the center of the chain at varying frequencies.

critical chain length, the chain rotates synchronously with the field. Once a chain is above the critical length at a particular frequency, its rotation becomes asynchronous. The solution decays asymptotically with increasing Mn. Additionally, we can define

$$l = [EI/(\zeta_\perp \omega)]^{1/2} \tag{21}$$

as the characteristic length scale associated with bending and drag. For $l/L \gg 1$, elasticity dominates and the chain is very rigid. For $l/L \ll 1$, viscous effects dominate and the rod bends to align along the axis of rotation and minimize its drag force. Longer chains are easier to bend. Also, the smaller the flexural rigidity, the less resistant the chain is to bending. From our previous bending experiments, we calculated that chains linked with PEG have a flexural rigidity between $EI \sim 10^{-21}$ N m^2 and $EI \sim 10^{-23}$ N m^2. Using these values, we can calculate the bounds of the critical chain length where viscous forces dominate and the chain bends, shown as dashed and dotted curves in Fig. 3(a). The filled circles on this plot show examples of the synchronous rotating chains we have studied while the open circles represent the asynchronous chains we have studied. We also plot the dependence of the phase lag angle on both chain length and frequency in Fig. 3(b). We note from Eq. (10) that the sine of the phase lag angle increases linearly with the angular velocity of a chain and more slowly with the chain length.

A. Synchronous rotating chains

For the most part, small chains ($N < 6$) will rotate synchronously as stable rigid rods where magnetic and elastic forces dominate over viscous forces. In this section, we will consider the more interesting case: chains rotating synchronously with the magnetic field where viscous forces dominate over elastic forces. Qualitatively, the initial response to low frequency rotations is for the chain to form S shapes to minimize drag and follow the external magnetic field. For chains with small deformations that rotate synchronously with the field, we determine the elastic force acting along the length of the chain by subtracting the radial magnetic force given by Eq. (17) from the viscous force given by Eq. (15) as described above. The elastic force increases linearly along the length of the chain corresponding to the higher velocity occurring at the outer ends of the chain. This causes the chain to bend in accordance with its elasticity. Using our previous micromanipulation results for the flexural rigidity of chains linked with PEG 733 and PEG 3400 as $EI \sim 10^{-21}$ N m^2 and $EI \sim 10^{-23}$ N m^2, respectively, we plot the model behavior with the experimental results as shown in Fig. 4 for PEG 733 and Fig. 5 for PEG 3400. The center of rotation does not always correspond to the center of the chain due to the fact that the chains are translating as well as rotating. For this reason, we find the center of rotation by examining the shape of the chain and finding the point of inflection in the curvature. We find that the PEG-linked chains rotate as bent flexible elastic rods with elastic properties that are well described by the measured flexural rigidity.

B. Asynchronous rotating chains

When the frictional torque exceeds the magnetic torque, the chain no longer synchronizes with the rotating external field. In the asynchronous regime, the phase lag angle of a rotating chain increases periodically with time as the chain rotates more slowly than the external magnetic field. As the phase lag angle α surpasses $\pi/2$, the chain slows down and reverses direction to realign its dipole moments with the external magnetic field. For chains where elastic forces are greater than viscous forces, this results in a chain that will rotate without a constant angular velocity in the rotating magnetic field as shown in Fig. 6(a). We show the orientation of the chain relative to the external magnetic field, which is shown by the solid arrow. Since the chain rotation is slow

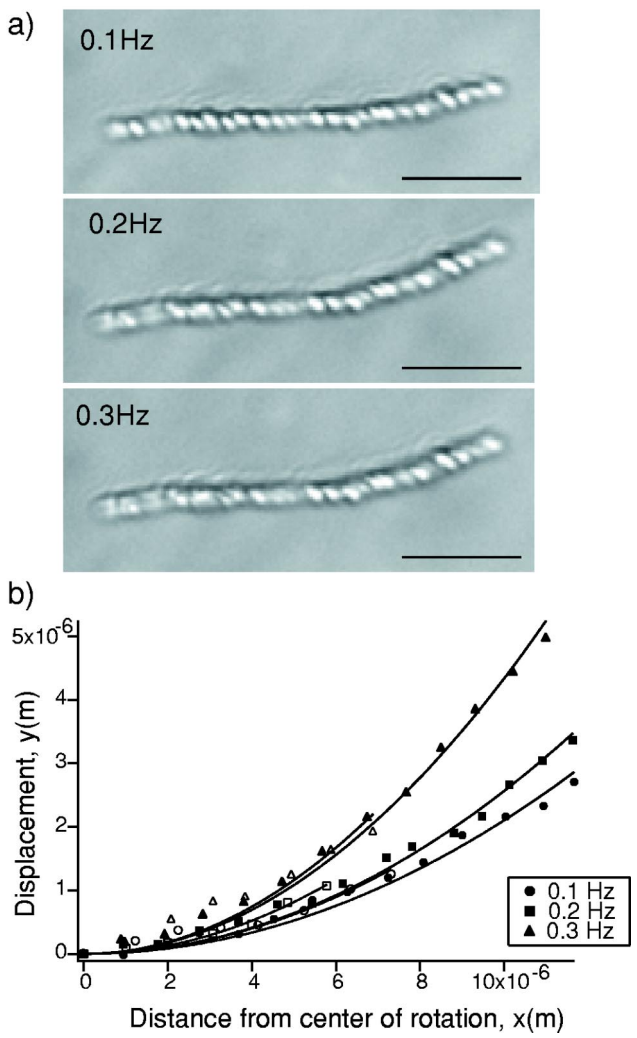

FIG. 4. (a) A chain linked with PEG 733 deforms as it rotates synchronously at various frequencies. (b) A plot of vertical displacement from center of rotation vs length from center at various frequencies. Filled markers represent the distance to the right of the center of rotation while open markers represent chain distance to the left of the center of rotation. The solid lines are calculations of deflection vs position for the different frequencies fitted to Eq. (20) using a flexural rigidity value of $EI \sim 10^{-21}$ N m^2. These fits compare the experimental results with model behavior. Scale bar: 10 μm.

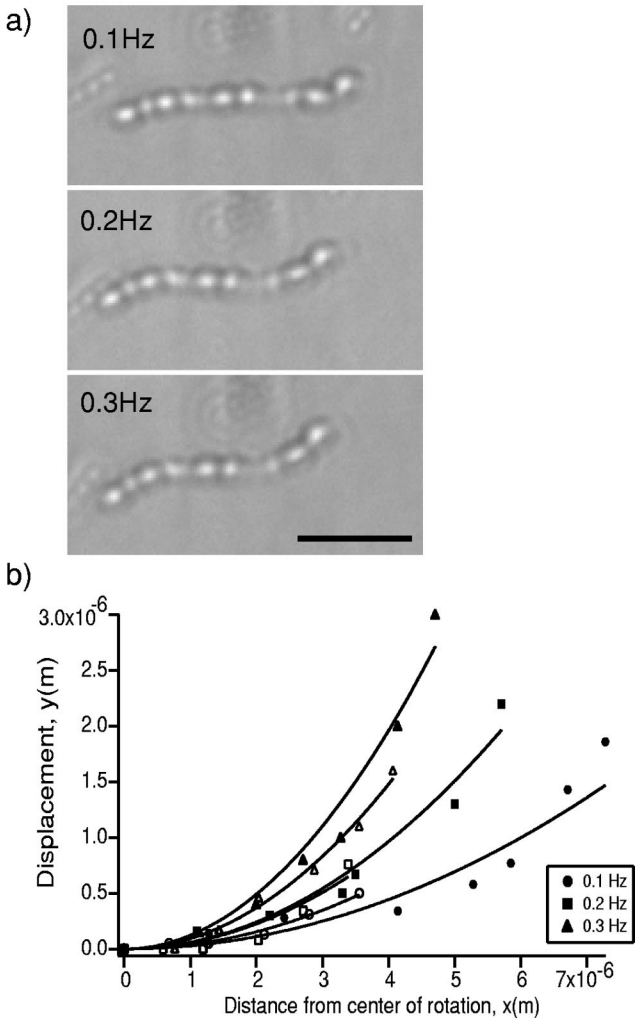

FIG. 5. (a) A chain linked with PEG 3400 deforms as it rotates synchronously at various frequencies. (b) A plot of vertical displacement from center of rotation vs length from center at various frequencies. Filled markers represent the distance to the right of the center of rotation while open markers represent chain distance to the left of the center of rotation. The deflection vs position for the different frequencies is fitted to Eq. (20) using a flexural rigidity value of $EI \sim 10^{-23}$ N m^2. These fits compare the experimental results with model behavior. Scale bar: 10 μm.

compared to the rotation of the field, the phase lag angle increases with time. The phase lag angle of the chain relative to the external magnetic field vs time is plotted in Fig. 6(b). We have also placed the lag of the chain dipole moment as shown by the crossed symbols. In the limit $\mathrm{Mn} \to \infty$, the magnetic rotation is faster than the chain response; thus the chain cannot move at very high frequencies.

When the viscous forces surpass the elastic forces, a chain will buckle. In this state the chain is both bent and compressed. It is well known that an elastic rod will exhibit Euler buckling when subjected to an external compressive force that exceeds a critical value,

$$F_{crit} = \frac{\pi^2 EI}{L^2}. \tag{22}$$

Once the compressive force is removed, the compressed rod will elastically recoil to a stable conformation. For a magnetic chain, lateral interactions between chain segments compete with these elastic restoring forces. The most common response of a PEG-linked chain upon the onset of buckling is to fold onto itself and rotate synchronously as a folded structure.

Gluteraldehyde chains buckle as they rotate. As shown in Fig. 7(a), a chain linked with gluteraldehyde follows the external magnetic field until $\alpha < \pi/4$. At that point the tension induced in the chain increases as the phase lag angle in-

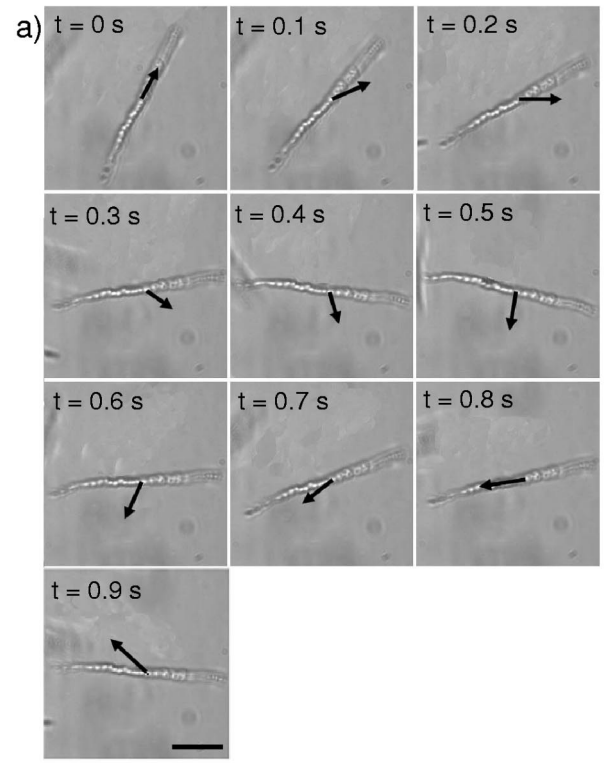

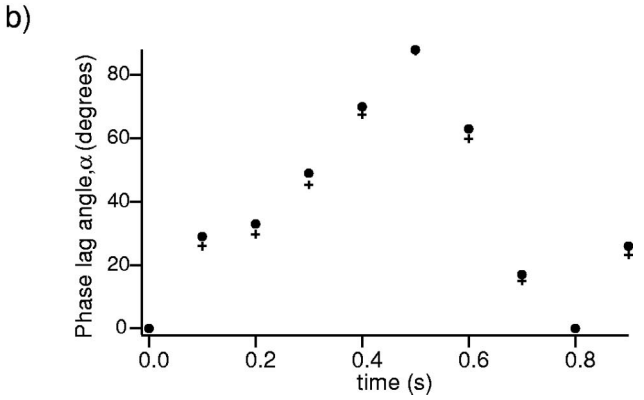

FIG. 6. (a) Video microscope images at 0.1 sec intervals of a glutaraldehyde-linked chain rotating asynchronously at 0.4 Hz. The external magnetic field direction is shown by black arrows. As the phase lag angle approaches 45°, the chain angular velocity slows. Once past 90°, the chain reverses direction until it realigns with the external field. Scale bar: 10 μm. (b) Plot of the phase lag angle with time. The chain phase lag angle is represented by filled circles while the crossed markers represent the phase lag angle of the dipole moment.

creases and the chain buckles. In this compressed state, the chain is elastically unstable. Eventually, the phase lag reaches $\pi/2$ and the chain reverses direction to align with the external field. At this point the chain straightens and releases tension once the dipole moments of the chain realign with the external field.

Several gluteraldehyde chains at various frequencies and lengths are studied. For a given frequency, we find the shortest chain length that has buckled. Longer chains will also buckle at the same force, but shorter chains will not. At the

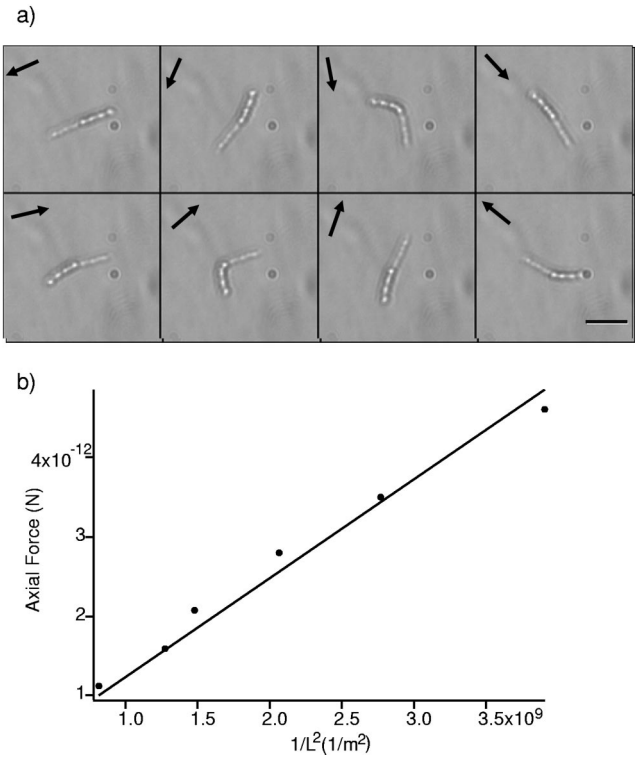

FIG. 7. (a) Video microscope images taken at 0.1 sec intervals of a chain linked with glutaraldehyde longer than the critical length. The external magnetic field direction is shown by black arrows. The chain bends to minimize its frictional torque but it is stiff enough to resist chain folding. This results in a chain that rotates asynchronously. Instead of rotating as a folded structure like PEG-linked chains, gluteraldehyde chains bend until the dipoles of the chain align with the external magnetic field and straighten once again. Scale bar: 5 μm. (b) A plot of axial load vs $1/L^2$ for glutaraldehyde-linked chains of various lengths.

given chain length and frequency, we calculate the tension and radial magnetic forces on a chain using Eqs. (15) and (17). Subtracting the radial magnetic force from the tension, we determine the axial load acting to compress the chain. A plot of the axial load vs $1/L^2$ is shown in Fig. 7(b). Using Eq. (22), the slope of this line gives a value $EI \sim 10^{-21}$ N m^2. This number is an order of magnitude smaller than that found in our micromanipulation experiments on gluteraldehyde-linked chains.

C. Synchronous rotating structures

The most common response of PEG-linked chains to a large buckling force is for the chain to buckle and fold as shown in Fig. 8(a). These structures continue to rotate synchronously with the external field as folded structure. We have observed a variety of collapsed structures, including chains that have folded into J and V shapes, as shown in Fig. 8(b). These structures have decreased their effective length to minimize the drag torque while observing magnetic and elastic restraints.

To understand the basic mechanism for these folded magnetic structures, we consider the magnetic interaction forces

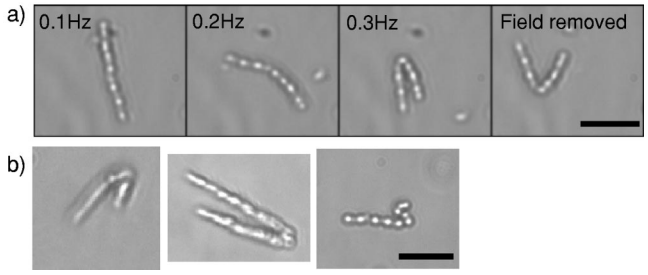

FIG. 8. (a) Video microscope images of a chain linked with PEG 3400 rotating at various frequencies. At 0.3 Hz, the chain folds and coalesces to rotate synchronously with the external magnetic field. Once the external magnetic field is removed, elastic recoil and thermal motion will cause the chain to open. (b) Variety of collapsed structures formed from initially straight chains at critical rotating frequencies. Scale bar: 5 μm.

between interacting segments of the chain. As a chain bends in response to a large compression force, segments of the chain are pushed more closely together leading to a magnetic interaction between folded segments.

Several groups have studied the lateral interaction between aligned dipoles and find long range attractions between fluctuating chains [16–20]. Among the observations, they find that fluctuating parallel dipolar chains will coalesce through a "zippering" motion [21]. The chains come in contact in one spot and cause the rest of the chain to come together.

The interaction energy between two rigid chains separated by a distance ρ is given by [20,22]

$$U_{chain} = (2\pi)^2 \frac{2m^2}{4\pi\mu_o \rho^2 a}\left(\frac{a}{\rho}\right)^{1/2} e^{-2\pi\rho/a}. \qquad (23)$$

Beyond a distance $\rho > 4a$, interaction energy is positive and the chains repel. When $\rho < 4a$, the interaction energy can be either positive or negative resulting in chains that are either repulsive or attractive depending on whether the particles in the parallel chains are in registry. Chains in registry repel one another, while chains staggered by $z = N/2$ are out of registry and attract one another.

For a linked chain to be able to fold, the total energy of the structure, which is the sum of the interaction energy and the deformation energy, $U = U_{chain} + U_{bend}$, must be minimized. As a chain buckles, the spacing between segments decreases which for staggered chain segments, reduces the energy of the structure. This decrease in chain energy works against the increased bending energy. This implies that the interaction force, $-\vec{\nabla} U_{chain}$, must be greater than the elastic bending force for a chain to remain folded.

To examine the interplay between these two forces, we examine the behavior of chains that unfold as the interaction energy is decreased. We begin with a chain that is rotating synchronously as a folded structure. As the field strength is slowly decreased there are changes in the bending curvature and spacing between chains as shown in Fig. 9(a). By measuring the distance between the folded arms of a chain at a given field strength, we can calculate the change in the magnetic interaction energy using Eq. (23) and compare it to the bending energy from Eq. (18): $U_{bend} = 1/2 EIL(d\Theta/ds)^2$. We determine the radius of curvature of the chains by fitting a circle of radius $(d\Theta/ds)^{-1}$. For the chain shown in Fig. 9, we see that at the lower field strengths, the bending energy dominates resulting in chains that are curved but not folded. At higher field strengths, the magnetic interaction energy between the arms of the chain becomes greater and the chain folds. The chain is stabilized in its bent form by the magnetic interaction forces between the folded arms of the chain.

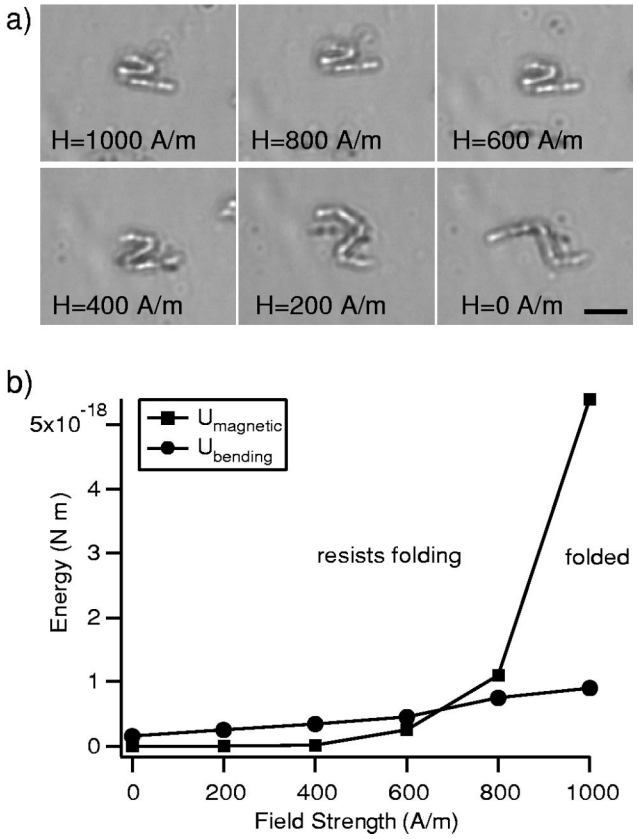

FIG. 9. (a) Video micrograph of a chain linked with PEG 3400 folded at 0.2 Hz, $H = 1000$ A/m. As the field strength is lowered, the chain begins to unfold. (b) Plot comparing the magnetic energy to the elastic bending energy at various field strengths. At low field strengths, the elastic bending energy dominates and the chain resists folding. At high field strengths, interchain energy dominates and the chain folds. Scale bar: 5 μm.

PEG-linked chains whose lengths are much greater than the critical chain length, bend in response to an increase in the viscous forces. These chains do not collapse into folded structures, instead they oscillate or "sway" back and forth as shown in Fig. 10. The phase lag angle for these chains increases and realigns with the external magnetic field more quickly than the lateral interaction forces can cause the chain to fold. Like the gluteraldehyde chains discussed previously, once the phase lag angle reaches $\pi/2$, the chain reverses direction in order to align with the external field and follow the field, resulting in a back and forth motion.

The starting configuration of a chain is another factor determining how it will rotate. Often, chains linked with PEG

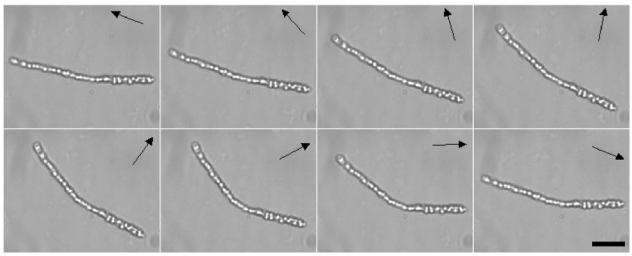

FIG. 10. Video micrograph showing that a long, 48 μm, chain linked with PEG 733 at 0.2 Hz cannot make a full rotation as it follows the external magnetic field shown by the black arrows. The chain lags behind the field until the phase lag becomes greater than 90°; the chain bends until it reverses directions to return to its starting point. This is because the magnetic field rotates at a rate that is much faster than the chain response rate. This results in a chain that "sways" back and forth. The time interval between each frame is 0.2 sec. The external magnetic field direction is shown by black arrows. Scale bar: 10 μm.

assume a curved configuration in the absence of any field. When placed in a rotating magnetic field, these structures often rotate without coalescing as shown in Fig. 11. Essentially, if the segments of the chain are in registry before the magnetic field is applied, these segments will repel each other once the magnetic field is applied creating a "stacked" structure that does not collapse.

V. CONCLUSION

Linked magnetic particles form novel MR materials that can be used to make magnetically actuated structures. By studying the differences in the mechanical properties of these chains we are able to understand how factors such as the flexibility of the spacer molecule or the length of the chain can affect their behavior under rotational fields. Specifically, the purpose of this work has been to examine chain response to a rotational magnetic field to compare the resulting shape to that predicted from a force balance. Our previous measurements of chain flexibility with optical tweezers provide excellent predictions of the shapes of synchronously rotating chains.

FIG. 11. PEG-linked chains that start as curved structures will rotate as folded shapes. (a) Chain linked with PEG 733 making a full rotation at 0.1 Hz. (b) Chain linked with PEG 3400 making a full rotation at 0.1 Hz. The time interval between each frame shown is 0.1 sec. The external magnetic field direction is shown by black arrows. Scale bar: 5 μm.

Additionally, we characterize the asynchronous rotation behavior and provide explanations of chain shape depending on chain length and magnetic field frequency. The main driving force is the minimization of the frictional torque the fluid exerts onto a chain balanced by the magnetic and elastic stability. A variety of shapes can be formed by PEG-linked chains, while those linked with gluteraldehyde rotate as rigid rods. Understanding the interplay between viscous, magnetic, and elastic forces allows us to control the shapes of rotating chains at various frequencies and rigidities.

ACKNOWLEDGMENT

This work was supported by the National Science Foundation Grant No. CTS-9980860.

[1] A. Margida, K. Weiss, and J. Carlson, Int. J. Mod. Phys. B **10**, 3335 (1996).
[2] I. Bica, J. Magn. Magn. Mater. **241**, 196 (2002).
[3] O. Sandre *et al.*, Phys. Rev. E **59**, 1736 (1999).
[4] S. Melle, G. G. Fuller, and M. A. Rubio, Phys. Rev. E **61**, 4111 (2000).
[5] G. Besseris, I. Miller, and D. Yeates, J. Rheol. **43**, 591 (1999).
[6] C. Wilhelm *et al.*, Phys. Rev. E **67**, 011504 (2003).
[7] S. Melle *et al.*, Int. J. Mod. Phys. B **16**, 2293 (2002).
[8] A. K. Vuppu, A. A. Garcia, and M. A. Hayes, Langmuir **19**, 8646 (2003).
[9] E. M. Furst *et al.*, Langmuir **14**, 7334 (1998).
[10] S. L. Biswal and A. P. Gast, Phys. Rev. E **68**, 021402 (2003).
[11] T. Deng *et al.*, Appl. Phys. Lett. **78**, 1775 (2001).
[12] M. Doi and S. F. Edwards, *The Theory of Polymer Dynamics* (Oxford University Press, New York, 1986).
[13] S. Melle and J. Martin, J. Chem. Phys. **118**, 9875 (2003).
[14] H. Zhang and M. Widom, Phys. Rev. E **51**, 2099 (1995).
[15] J. Martin and R. Anderson, J. Chem. Phys. **104**, 4814 (1996).
[16] J. Martin, J. Odinek, and T. Halsey, Phys. Rev. Lett. **69**, 1524 (1992).
[17] J. Martin *et al.*, Phys. Rev. E **57**, 756 (1998).
[18] A. Silva *et al.*, Phys. Rev. E **54**, 5502 (1996).
[19] M. Hagenbuchle and J. Liu, Appl. Opt. **36**, 7664 (1997).
[20] E. M. Furst and A. P. Gast, Phys. Rev. E **62**, 6916 (2000).
[21] M. Fermigier and A. P. Gast, J. Colloid Interface Sci. **154**, 522 (1992).
[22] T. Halsey, Science **258**, 761 (1992).